

# Expectile Periodograms

Tianbo Chen<sup>1</sup>

---

## Abstract

In this paper, we introduce a novel periodogram-like function called expectile periodograms, for detecting and estimating hidden periodicities in time series. The expectile periodograms are constructed from trigonometric expectile regression, in which a specially designed objective function is used to substitute the squared  $l_2$  norm that leads to the ordinary periodograms. Analogous to quantile periodograms, the expectile periodograms provide a broader view of the time series than the ordinary periodograms by examining different expectile levels, while achieving higher computational efficiency. Simulations demonstrate the efficiency and robustness of the expectile periodograms in the presence of hidden periodicities. Finally, we leverage the inherent two-dimensional characteristics of the expectile periodograms and train a deep-learning (DL) model to classify the earthquake waveform data. Remarkably, our approach achieves higher classification testing accuracy when juxtaposed with alternative periodogram-based methodologies.

*Keywords:* Periodogram; Expectile regression; Spectral density; Time series analysis

---

## 1. Introduction

Spectral density functions (SDFs) constitute an important element within time series analysis, where data are analyzed in the frequency domain. The ordinary eriodograms, a raw non-parametric estimator of the SDF, are widely

---

<sup>1</sup>Anhui University, China. E-mail: chentianbo@ahu.edu.cn

used in many applications. A notable instance of its deployment is in Electroencephalogram (EEG) data analysis, where the spectral features revealed by the ordinary periodograms are used for disease diagnosis (Polat and Güneş, 2007; Baud et al., 2018; Martínez-Murcia et al., 2019). Furthermore, the ordinary periodograms find utility in EEG channel clustering (Euán et al. (2018); Maadooliat et al. (2018); Chen et al. (2021a)). Ordinary periodograms are construed by the ordinary least squares (OLS) regression on the trigonometric regressor, which is primarily focused on the conditional mean. Consequently, the ordinary periodograms may exhibit limitations in terms of robustness and effectiveness, particularly in handling data with asymmetric or heavy-tailed distributions (Bloomfield, 2004).

An alternative regression approach is quantile regression, which evaluates the variation of the conditional quantiles with respect to the response variable. The pioneering work of Koenker and Bassett Jr (1978) introduced the concept of quantile regression and the methodology has been comprehensively extended by Koenker (2005). For a detailed and systematic introduction to quantile regression and its interesting extensions, we refer to Kouretas et al. (2005); Cai and Xu (2008); Cai and Xiao (2012); Koenker (2017). Armed with a specially designed loss function, quantile regression not only provides a more complete picture of the relationship between the response variable and the covariates, but also shows strong robustness against outliers. Quantile regression techniques have been applied in various fields (Garcia et al., 2001; Machado and Mata, 2005; Alvarado et al., 2021; Sharif et al., 2021). An innovative development is the quantile periodogram (Li, 2012b) constructed by trigonometric quantile regression, which demonstrates its ability to detect hidden periodicities in time series. Similarly to the behavior of the ordinary SDFs and periodograms, the quantile periodograms are unbiased estimators of the so-called quantile spectrum, which are scaled versions of the ordinary SDFs of the level-crossing process. Notably, the Laplace periodograms (Li, 2008) represented a specialized case of the quantile periodograms when the quantile is set to 0.5. Related works on quantile periodograms include Li (2012a); Hagemann (2013); Li (2014); Dette

et al. (2015); Kley (2016); Birr et al. (2017); Meziani et al. (2020); Chen et al. (2021b); Li (2023).

However, quantile regression is beset by several limitations. First, it has a heightened computational burden due to the non-differentiability of the loss function. Second, quantile regression is less effective for light-tailed noise. Third, the uniqueness of the solution is not guaranteed. To balance robustness and effectiveness and address these shortcomings, the concept of expectile regression has been proposed. The asymmetric least square (ALS) regression, also known as expectile regression, was proposed in Newey and Powell (1987). While quantile regression can be regarded as a generalization of median regression, expectile regression can be seen as a combination of the OLS regression and quantile regression. Expectile regression exhibits the ability to measure the whole distribution of the data and is much easier to compute using quadratic optimization. A comprehensive comparative analysis of quantiles and expectiles is presented in Waltrup et al. (2015), wherein the relationships between these two approaches are thoroughly examined. Jones (1994) provided mathematical proof that expectiles indeed correspond to quantiles of a distribution function uniquely associated with the underlying data distribution. Building on this foundation, Yao and Tong (1996) established the existence of a bijective function that directly relates expectiles to quantiles, thereby facilitating the calculation of one from the other. Alternative approaches for estimating quantiles from expectiles are introduced in Efron (1991); Granger and Sin (1997); Schnabel and PHC (2009), elucidating methodologies for estimating the density (and also, quantiles) from a set of expectiles by using penalized least squares. As a generalization of quantile regression and expectile regression, Jiang et al. (2021) introduce the  $k$ -th power expectile regression with  $1 < k \leq 2$ .

Expectile regression techniques have found applicability across diverse domains. Jiang et al. (2017) introduced an expectile regression neural network (ERNN) model. This novel approach incorporates a neural network structure into expectile regression, thereby facilitating the exploration of potential nonlinear relationships between covariates and the expectiles of the response variable.

Gu and Zou (2016) systematically studied the Sparse Asymmetric Least Squares (SALES) regression under high dimensions where the penalty functions include the Lasso and nonconvex penalties. Xu et al. (2020) developed a novel mixed data sampling expectile regression (MIDAS-ER) model to measure financial risk and demonstrated exceptional performance when applied to two popular financial risk measures: Value at Risk (VaR) and Expected Shortfall (ES). Another approach by Xu involved the elastic-net penalty into expectile regression, and applied the model to two real-world applications: relative location of CT slices on the axial axis and metabolism of tacrolimus drug.

Inspired by the notable success achieved through expectile regression and the pioneer foundation of the quantile periodograms, we employ expectile regression to define a novel spectral estimator termed the expectile periodograms, for spectral analysis of time series data. In this paper, we demonstrate that the expectile periodograms not only share similar properties of the ordinary periodograms as a frequency-domain representation of serial dependence within the time series, but also offer a more comprehensive understanding of the time series across the entire range of the expectile levels. The rest of the paper is organized as follows. In Section 2, we define the expectile periodograms and make a comparison to the ordinary and quantile periodograms. In Section 3, we present comparative studies on the performances of the different periodograms by simulations. In Section 4, we apply our method to a time-series classification task. We take advantage of the two-dimensional property of the expectile periodograms and train a deep-learning (DL) model to classify the earthquake data. The conclusion and future work are discussed in Section 5.

## 2. Expectile Periodograms

In this section, we define the expectile periodograms and demonstrate their capability in detecting hidden periodicities through two time series examples.

For a real-valued time series  $\{Y_1, Y_2, \dots, Y_n\}$ , the ordinary periodogram, which

serves as a raw estimator of the spectral density, is defined as:

$$I_n(\omega) = \frac{1}{n} \left| \sum_{t=1}^n Y_t e^{-jt\omega} \right|^2, \quad (1)$$

where  $\omega \in (0, \pi)$ . Then, when  $\omega$  takes value at the Fourier frequencies:  $\omega_j = 2\pi j/n, j = 1, \dots, [n/2]$ , the ordinary periodogram can also be expressed as:

$$I_n(\omega) := \frac{1}{4} n \|\bar{\beta}_n(\omega)\|_2^2, \quad (2)$$

where  $\bar{\beta}_n(\omega)$  is obtained via the ordinary least squares (OLS):

$$\bar{\beta}_n(\omega) = \arg \min_{\beta \in \mathbb{R}^2, \mu \in \mathbb{R}} \sum_{t=1}^n \{Y_t - \mathbf{x}_t^\top(\omega)\beta(\omega)\}^2,$$

with the trigonometric regressor  $\mathbf{x}_t(\omega) = \{\cos(\omega t), \sin(\omega t)\}^\top$ .

The equivalence of (1) and (2) can be directly established by the Fourier representation of  $\{Y_t\}$ :

$$Y_t = \lambda + \sum_{l=1}^q \cos(\omega_j t) + \sin(\omega_j t),$$

where  $\lambda$  is a suitable constant.

OLS techniques focus on the conditional mean of the response variable given the predictors. In contrast, expectile regression offers a more comprehensive perspective of the data by exploring a range of expectile levels, thus providing insight into different aspects of the distribution of the response. Moreover, expectile regression demonstrates robustness against asymmetrically distributed noise and nonlinear distortions. In this work, we introduce the expectile periodograms, extending the ordinary periodograms by replacing the OLS regression with expectile regression.

Given an expectile level  $\tau \in (0, 1)$ , the asymmetric least squares (ALS) (Newey and Powell, 1987) cost follows

$$\rho_\tau(u) = |\tau - I(u < 0)| \cdot u^2,$$

where  $I(\cdot)$  denotes the indicator function. Consider the linear trigonometric expectile regression solution:

$$\hat{\beta}_{n,\tau}(\omega) = \arg \min_{\beta \in \mathbb{R}^2, \lambda_\tau \in \mathbb{R}} \sum_{t=1}^n \rho_\tau\{Y_t - \lambda_\tau - \mathbf{x}_t^\top(\omega)\beta(\omega)\}, \quad (3)$$

where  $\lambda_\tau$  is a suitable constant, typically the  $\tau$ -expectile of  $\{Y_t\}$  given by:

$$\lambda_\tau = \arg \min_{\lambda \in \mathbb{R}} \sum_{t=1}^n \rho_\tau(Y_t - \lambda),$$

and  $\boldsymbol{\beta}(\omega) = [\beta_1(\omega), \beta_2(\omega)]^\top$ . The normalized frequency  $f = \omega/2\pi \in (0, 1/2)$ , which denotes the number of cycles per unit time, is used in the figures throughout the remainder of the paper for illustration. Aigner et al. (1976) showed that  $\hat{\boldsymbol{\beta}}_{n,\tau}(\omega)$  can be interpreted as a maximum likelihood estimator when the disturbances arise from a normal distribution with unequal weight placed on positive and negative disturbances.

Then, we define the expectile periodograms at expectile level  $\tau$  as:

$$EP_{n,\tau}(\omega) := \frac{1}{4}n\|\hat{\boldsymbol{\beta}}_{n,\tau}(\omega)\|_2^2 = \frac{1}{4}n\hat{\boldsymbol{\beta}}_{n,\tau}^\top(\omega)\hat{\boldsymbol{\beta}}_{n,\tau}(\omega).$$

In other words, the expectile periodogram is a scaled version of the squared norm of the expectile regression coefficients corresponding to the trigonometric regressor  $\mathbf{x}_t(\omega)$ . While the parameter  $\lambda_\tau$  is fixed in (3), it can also be optimized alongside with  $\boldsymbol{\beta}(\omega)$  to obtain the extended expectile regression solution:

$$\{\hat{\lambda}_\tau(\omega), \hat{\boldsymbol{\beta}}_{n,\tau}(\omega)\} := \arg \min_{\boldsymbol{\beta} \in \mathbb{R}^2, \lambda_\tau \in \mathbb{R}} \sum_{t=1}^n \rho_\tau\{Y_t - \lambda_\tau - \mathbf{x}_t^\top(\omega)\boldsymbol{\beta}(\omega)\}.$$

Quantile regression also provides richer information than OLS by examining the time series at different quantile levels, but it is less computationally efficient compared to expectile regression. Li (2012b) proposed the quantile periodograms by replacing the OLS estimator in (2) with the quantile regression estimator:

$$\tilde{\boldsymbol{\beta}}_{n,\alpha}(\omega) := \arg \min_{\boldsymbol{\beta} \in \mathbb{R}^2, \lambda_{\tau\alpha} \in \mathbb{R}} \sum_{t=1}^n \rho_\alpha^*\{Y_t - \lambda_\alpha - \mathbf{x}_t^\top(\omega)\boldsymbol{\beta}(\omega)\},$$

where  $\rho_\alpha^*(u) = u\{\alpha - I(u < 0)\}$ . Then, the quantile periodogram at quantile level  $\alpha \in (0, 1)$  is defined as

$$QP_{n,\alpha}(\omega) := \frac{1}{4}n\|\tilde{\boldsymbol{\beta}}_{n,\alpha}(\omega)\|_2^2 = \frac{1}{4}n\tilde{\boldsymbol{\beta}}_{n,\alpha}^\top(\omega)\tilde{\boldsymbol{\beta}}_{n,\alpha}(\omega). \quad (4)$$

With  $\alpha = 0.5$ , the quantile periodograms reduce to the Laplace periodograms introduced in Li (2008).

### 2.1. Examples

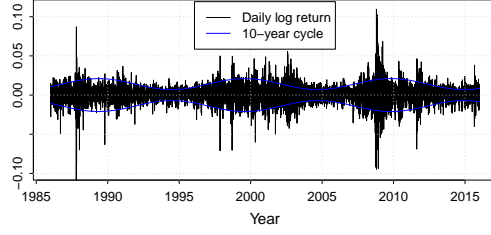
While the expectile periodograms can be examined at a specific expectile level like the ordinary periodogram, they can also be analyzed as bivariate functions of parameters  $\tau$  and  $\omega$ , providing a much richer view of the time series. To illustrate such duality, we consider two time series examples in different scientific fields, in which the ordinary periodograms fail to detect hidden periodic patterns. Noticed that the main purpose of this paper is to analyze the serial dependence of the time series, with amplitude considerations being of secondary importance. Therefore, for the remainder of the paper, we normalize the periodograms at each expectile level such that the summation over  $\omega$  equals 1.

In the first example, we analyze the daily log returns of the S&P 500 Index data from 1986 to 2015, shown in Figure 1(a). The expectile periodograms in Figure 1(b) successfully identify the 10-year cycle of market volatility (highlighted by the blue lines in Figure 1(a)) at both the lower and upper expectiles. In contrast, the ordinary periodogram yields a relatively featureless flat line. The smoothed periodograms in Figure 1(d) and (e), obtained using the `smooth.spline` function in R with the tuning parameter selected by generalized cross-validation (GCV), display a spectral feature similar to a GARCH(1,1) (Bollerslev, 1986) process:  $Y_t \sim N(0, \sigma_t^2)$ ,  $\sigma_t^2 = 10^{-6} + 0.35Y_{t-1}^2 + 0.35\sigma_{t-1}^2$  ( $t = 1, \dots, 200$ ). The periodograms for this GARCH(1,1) process are shown in Figure 1(f) and (g). Notably, while the ordinary periodogram of GARCH(1,1) model is a constant, the expectile periodograms detect the low-frequency feature at both the lower and higher expectiles.

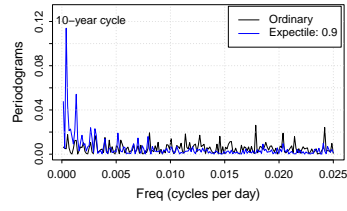
The second example is based on EEG data collected from an epilepsy patient during a seizure interval <sup>2</sup>. In Figure 2(a), the EEG segments and corresponding sample expectiles are displayed. The ordinary periodogram in Figure 2(b) successfully detects both low-frequency and high-frequency components, which correspond to the six main spikes and the associated bursts, respectively. The

---

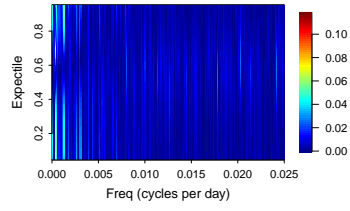
<sup>2</sup>The data was collected by South China Normal University School of Psychology and is authorized for use in this paper.



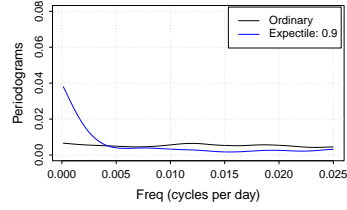
(a)



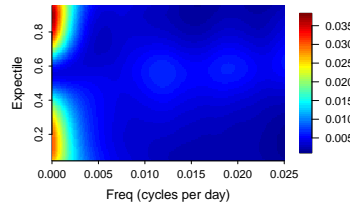
(b)



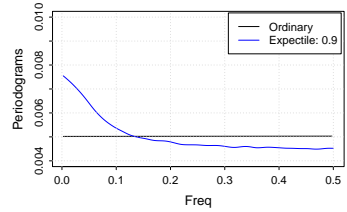
(c)



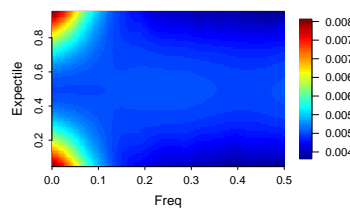
(d)



(e)



(f)



(g)

Figure 1: (a) Daily log returns of the S&P 500 Index data; (b) the ordinary periodogram and the expectile periodogram at  $\tau = 0.9$ ; (c) the expectile periodogram at expectiles  $\{0.05, 0.06, \dots, 0.95\}$ ; (d) and (e) the smoothed versions of (b) and (c), respectively; (f) the ordinary periodogram and the expectile periodogram of the GARCH(1,1) model at  $\tau = 0.9$ ; and (g) the expectile periodogram of the GARCH(1,1) model at expectiles  $\{0.05, 0.06, \dots, 0.95\}$ . (f) and (g) are obtained by the averages of 5000 Monte Carlo simulation runs.



expectile periodograms in Figure 2(b) and (c) provide further insights, revealing that the high-frequency patterns appear predominantly at higher expectile levels. This phenomenon aligns with the EEG data, as the bursts occur mainly at the peaks of the main spikes. Furthermore, the intensity of the bursts increases with higher expectiles, particularly at frequencies  $\omega \in [0.02, 0.03]$ , as shown in Figure 2(d).

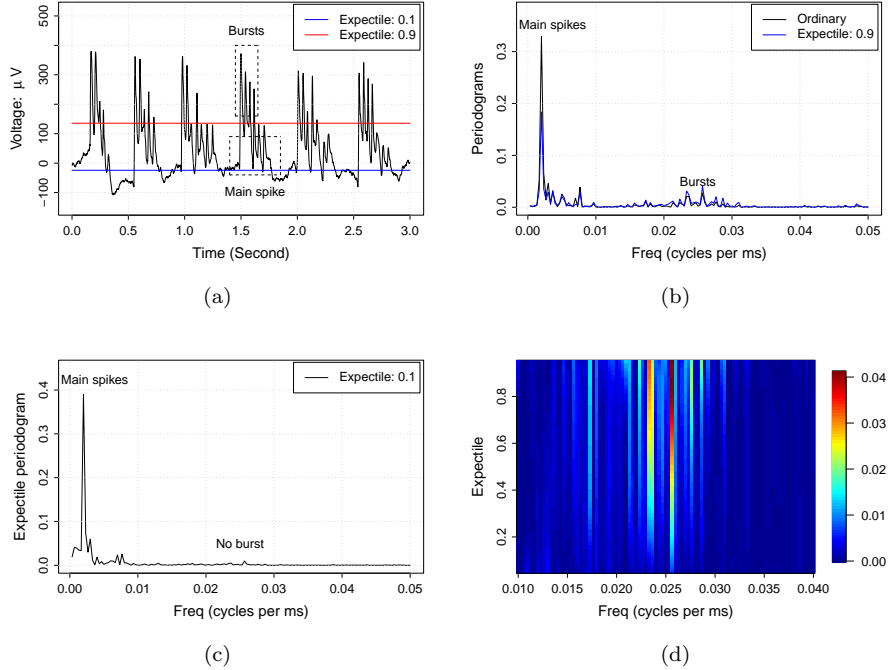


Figure 2: (a) The EEG data over a 3-second interval, along with its sample expectiles levels 0.1 and 0.9; (b) the ordinary periodogram and the expectile periodogram at  $\tau = 0.9$ ; (c) the expectile periodogram at  $\tau = 0.1$ ; and (d) the expectile periodogram at expectiles  $\{0.05, 0.06, \dots, 0.95\}$ . The time resolution of the EEG data is 1000Hz.

### 3. Numerical Results

In this section, we present numerical results to demonstrate the efficiency of the expectile periodograms in detecting hidden periodicities in time series.

### 3.1. Hidden Periodicities Detection

We consider the following model:

$$Y_t = a_t X_t, \tag{5}$$

where

$$a_t = b_0 + b_1 \cos(\omega_0 t) + b_2 \sin(\omega_1 t),$$

with  $b_0 = 1, b_1 = 0.9, b_2 = 1$ .  $\{X_t\}$  is an AR(2) process satisfying

$$X_t = \phi_1 X_{t-1} + \phi_2 X_{t-2} + \epsilon_t, \tag{6}$$

with  $\phi_1 = 2r \cos(\omega_c), \phi_2 = -r^2$  ( $r = 0.6$ ) and  $\{\epsilon_t\}$  is the noise. Additionally, we set  $\omega_0 = 0.1 \times 2\pi, \omega_1 = 0.12 \times 2\pi$ , and the parameter  $\lambda_\tau$  is taken to be the sample  $\tau$ -expectile of  $\{Y_t\}$ . This setup aims to evaluate the effectiveness of different types of periodograms in detecting multiple closely spaced periodicities.

The expectile periodograms can serve as representations of serial dependence in the frequency domain of the time series when no hidden periodicities are present. We first present the periodograms of model (6) with  $\omega_c = 2\pi \times 0.25$  and  $2\pi \times 0.3$ . As shown in Figure 3 (a) and (b), the ordinary periodograms, the expectile periodograms and the Laplace periodograms, exhibit a similar bell-shaped pattern with a spectral peak around  $\omega_c$ . The results is expected for the spectral densities of the AR(2) process. The characteristic polynomial of (6) is  $\phi(z) = 1 - \phi_1 z - \phi_2 z^2$ , where the roots  $z_1$  and  $z_2$  are complex conjugates, with magnitude  $|z_1| = |z_2| = 1/r > 1$ , ensuring causality. The AR coefficients  $\phi_1$  and  $\phi_2$  determine the location and narrowness of the spectral peak. Specifically, the peak frequency is positioned  $\omega_c/2\pi$  and as  $r \rightarrow 1^-$ , the peak becomes narrower (Shumway and Stoffer, 2016). Figure 3 (c) and (d) show the expectile periodograms at expectiles  $\{0.05, 0.06, \dots, 0.95\}$ , which share similar features to the quantile spectrum in Chen et al. (2021b). Specifically, all periodograms shown are ensemble means of 5000 smoothed periodograms.

Figure 4 demonstrates the ability of the expectile periodograms to detect hidden periodicities. We present the mean of 5000 realizations of the ordinary

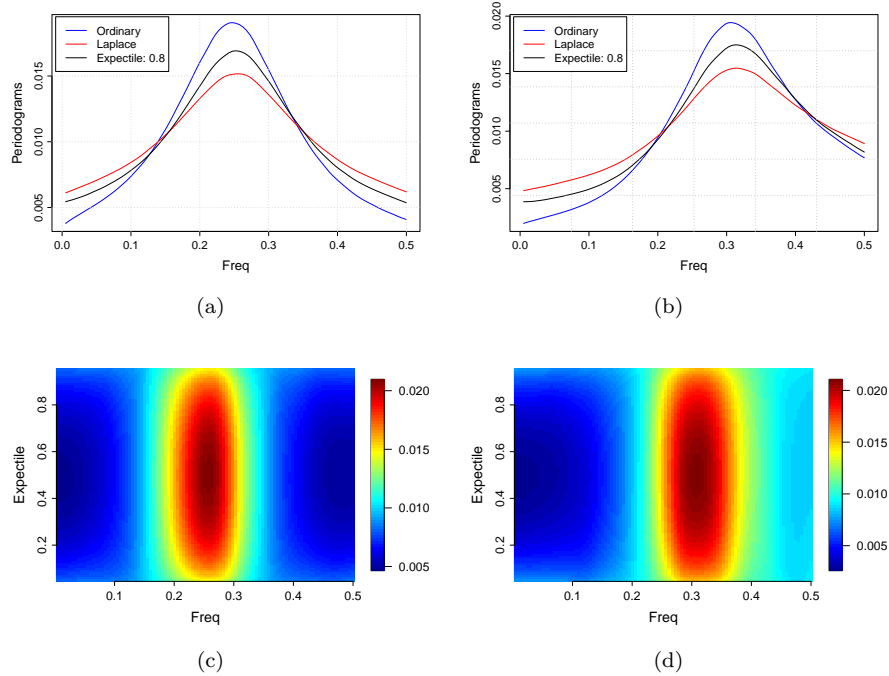


Figure 3: Ensemble means of three types of smoothed periodograms of time series defined by model (6) with standard Gaussian white noise. (a) The three periodograms with  $\omega_c = 2\pi \times 0.25$ , (b) the three periodograms with  $\omega_c = 2\pi \times 0.3$ , (c) and (d) the expectile periodograms at expectiles  $\{0.05, 0.06, \dots, 0.95\}$  for  $\omega_c = 2\pi \times 0.25, 0.3$ , respectively. The number of realizations is 5000 and the sample size  $n = 200$ .

and the expectile periodograms of model (5). The expectile periodograms detect the hidden periodicities as large spikes at  $\omega_0$  and  $\omega_1$ , whereas the ordinary periodograms do not exhibit this capability. It is important to note that spectral leaks, which have been observed for the Laplace periodograms, can also occur in the expectile periodograms. Therefore, small spikes may take place at some other frequencies, as indicated by Theorem 2 in Li (2012b). To mitigate the issue of spectral leakage, incorporating an  $l_1$  regularization into the loss function is helpful (Meziani et al., 2020).

The expectile periodograms in Figure 2(g) and 3 are symmetric across the expectile levels. To demonstrate the capability of the expectile periodograms to

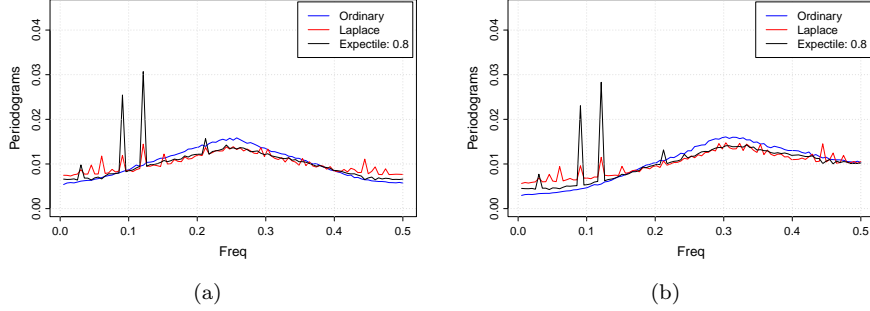


Figure 4: Means of the three types of periodograms of time series defined by model (5). (a) Represents  $\omega_c = 0.25$  and (b) with  $\omega = 0.3$ , respectively. The number of realizations is 5000 and the sample size  $n = 200$ .

handle more complex spectral features, we construct  $Y_t$ , whose expectile periodograms are asymmetric across the expectile levels.  $Y_t$  defined as a nonlinear mixture of three components:

$$Z_t = W_1(X_{t1}) X_{t1} + \{1 - W_1(X_{t1})\} X_{t2},$$

$$Y_t = W_2(Z_t) Z_t + \{1 - W_2(Z_t)\} X_{t3}. \quad (7)$$

The components  $\{X_{t1}\}$ ,  $\{X_{t2}\}$ , and  $\{X_{t3}\}$  are independent Gaussian AR(1) processes satisfying

$$X_{t1} = 0.8X_{t-1,1} + w_{t1},$$

$$X_{t2} = -0.75X_{t-1,2} + w_{t2},$$

$$X_{t3} = -0.81X_{t-2,3} + w_{t3},$$

where  $w_{t1}, w_{t2}, w_{t3}$  are standard Gaussian white noise. From the perspective of traditional spectral analysis, the series  $\{X_{t1}\}$  has a lowpass spectrum,  $\{X_{t2}\}$  has a highpass spectrum, and  $\{X_{t3}\}$  has a bandpass spectrum around frequency  $1/4$ . The mixing function  $W_1(x)$  is equal to 0.9 for  $x < -0.8$ , 0.25 for  $x > 0.8$ , and linear transition for  $x$  in between. The mixing function  $W_2(x)$  is similarly defined except that it equals 0.5 for  $x < -0.4$  and 1 for  $x > 0$ . Figure 5 shows the expectile periodograms of model (7), where the expectile periodogram

is asymmetric across the expectile levels. It is noteworthy that the ordinary periodograms can only analyze spectral features near the middle expectiles, while the expectile periodograms offer a more comprehensive understanding of the time series across the entire range of  $\tau \in (0, 1)$ .

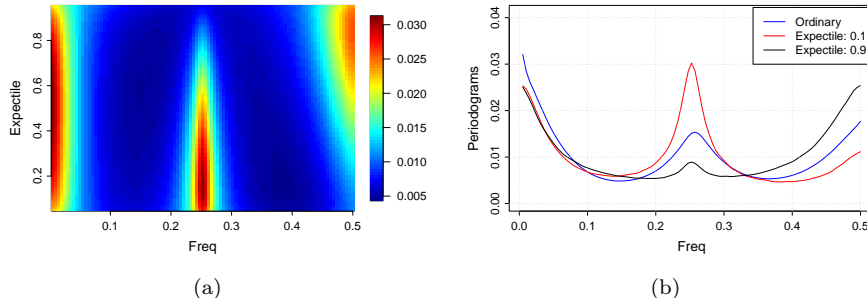


Figure 5: The periodograms of the mixture model defined by model (7). (a) The expectile periodogram with asymmetric pattern across the expectile level, and (b) the expectile periodograms at extreme expectiles ( $\tau = 0.1$  and  $0.9$ ), as well as the ordinary and the Laplace periodograms. The number of realizations is 5000 and the sample size  $n = 200$ .

### 3.2. Fisher's Test

One commonly used hypothesis test for detecting periodicities for the ordinary periodograms is Fisher's test (Brockwell and Davis, 1991). For frequencies  $\omega = \{\omega_1, \omega_2, \dots, \omega_l\}$ , the test statistic is defined by

$$g = \frac{\max_{1 \leq k \leq l} \{I_n(\omega_k)\}}{\sum_{k=1}^l I_n(\omega_k)}. \quad (8)$$

Fisher's test implies the presence of hidden periodicity if  $g$  is sufficiently large. The null hypothesis is that the time series is Gaussian white noise, while the alternative hypothesis is that the time series contains a deterministic periodic component of unspecified frequency.

We apply Fisher's test to the expectile periodograms by replacing  $I_n(\omega)$  with  $EP_{n,\tau}(\omega)$ . The probabilities of detection are obtained by Monte Carlo simulation runs for time series defined by model (5), with a single periodicity with  $\omega_0 = 0.1 \times 2\pi$ ,  $\omega_c = 0.3 \times 2\pi$ , and  $b_2 = 0$ . The results are shown in

Table 1. Both the expectile and quantile periodograms outperform the ordinary periodograms. At a significance level of 0.05, the expectile periodogram ( $\tau = 0.9$ ) achieves the detection rate of 84.26%, whereas the ordinary periodogram only achieves 29.78%. The detection rates vary depending on the expectile level. In this experiment, as the expectile or quantile approaches to 1, the detection rate of the expectile periodograms shows an increasing trend and surpasses that of the quantile periodograms.

Table 1: Fisher’s test of different types of periodograms.

Significa- nce level	Expectile periodograms			Quantile periodograms			Ordianry p- eriodograms
	$\tau=0.85$	$\tau=0.9$	$\tau=0.95$	$\alpha=0.85$	$\alpha=0.9$	$\alpha=0.95$	
0.01	0.4048	0.5608	0.5850	0.6898	0.6328	0.4428	0.1224
0.05	0.7158	0.8426	0.8510	0.8720	0.8260	0.6646	0.2978
0.10	0.8308	0.9262	0.9306	0.9278	0.8952	0.7678	0.4258

### 3.3. Smoothed Expectile Periodograms

The power spectrum can be estimated consistently by a properly smoothed ordinary periodogram Brockwell and Davis (1991). However, the absence of analytical expressions for the mean and variance of the expectile periodograms makes it difficult to conduct a similar investigation. To address this, we employ simulations to demonstrate that the distance between the smoothed expectile periodograms and the ground truth (averaged expectile periodograms of 50,000 realizations) decreases as  $n$  increases. We use models (6) and (7) at  $\tau = 0.9$  for illustration.

We measure the distance using both the mean squared error (MSE) and Kullback-Leibler (KL) divergence (Kullback and Leibler, 1951). Figure 6 depicts the MSE and KL divergence as a function of  $n$ , with  $n$  taking values of 200, 400, 800, and 1600. To highlight the decreasing trend as  $n$  increases, the values are normalized by setting the maximum to 1.

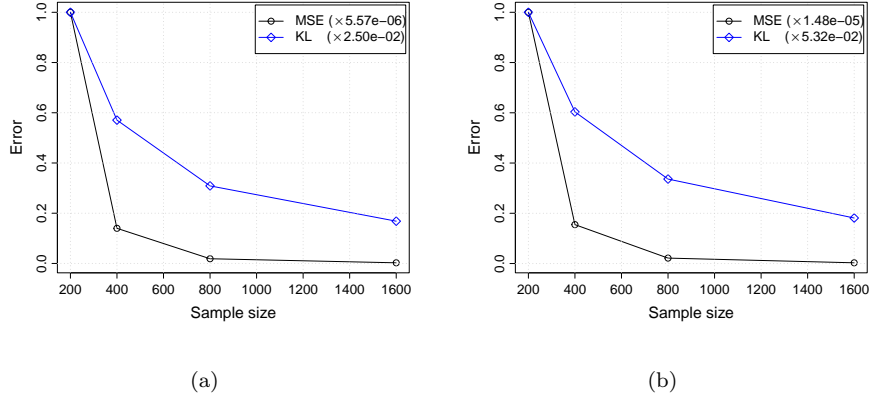


Figure 6: MSE and KL divergence of smoothed periodograms. (a) AR(2) model (6); (b) mixture model (7). The results are based on 5000 simulation runs.

#### 4. Earthquake Data Classification

In this section, we apply the expectile periodograms to an earthquake classification problem. Section 4.1 provides an introduction to the earthquake data, while Section 4.2 describes the deep learning model and presents the classification results.

##### 4.1. Data Description

The earthquake waveform data with a sampling rate of 100 Hz, was collected in February 2014 in Oklahoma State. This data is available at <https://www.iris.edu/hq/> and <http://www.ou.edu/ogs.html>. Details about the catalog data are provided in Benz et al. (2015), which includes labels for the magnitudes and times of the earthquakes. We extract 2000 non-overlapping segments of data, each being a time series with  $n = 2000$ , equivalent to 20 seconds of data. The choice of longer time series ensures that the segments contain complete earthquake events. Among these segments, 1000 of them contain an earthquake with magnitudes greater than 0.25, while the remaining 1000 segments contain no earthquakes. We smooth the expectile periodograms of the 2000 segments using the semi-parametric method proposed in Chen et al.

(2021b), ensuring smoothness across both expectile and frequency dimensions. In this experiment, we use the lower half of the frequencies ( $\omega \leq 0.25 \times 2\pi$ ) and 46 expectiles (0.05, 0.07, ..., 0.93, 0.95). Since we focus on serial dependence and normalize the expectile periodograms, amplitude considerations are excluded, which makes the classifications more challenging. Additionally, we incorporate two competitive periodograms: the smoothed ordinary periodogram and the quantile periodogram.

We show three representative segments along with their corresponding smoothed expectile periodograms in Figure 7. Specifically, Figure 7(a) contains a large earthquake with a magnitude larger than 3, Figure 7 (b) contains a somehow small earthquake with a magnitude less than 1, and Figure 7 (c) contains no earthquake. Based on the three segments, we have the following features:

- The smoothed expectile periodograms for the segment with a large earthquake exhibit spectral peaks at the low-frequency band in both the higher and lower expectiles.
- The smoothed expectile periodograms for the segment with a small earthquake exhibit spectral peaks at both the low-frequency band (both the lower and higher expectiles) and the high-frequency band (middle expectiles).
- The smoothed expectile periodograms for the segment with no earthquake only exhibit peaks at the high-frequency bands.

#### 4.2. Classification using Deep Learning Model

In this section, we use the three types of smoothed periodograms as features to classify the segments into those that contain earthquakes and those that do not. We randomly split the segments into training and testing sets, comprising 1600 and 400 samples, respectively.

To classify the expectile periodograms and the quantile periodograms, we employ a model with two convolutional layers for feature extraction, each followed by a max-pooling layer. The second pooling layer connects to a fully



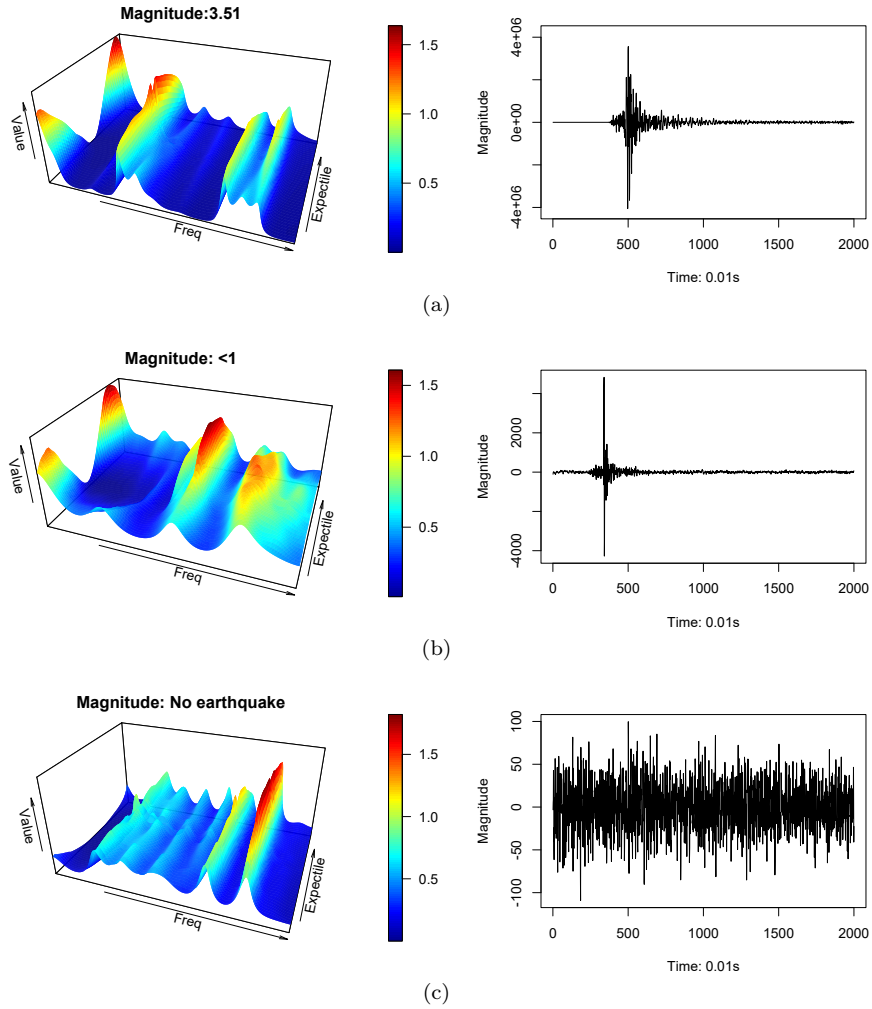


Figure 7: Three segments and the corresponding smoothed expectile periodograms. (a) The segment with an earthquake with a magnitude  $> 3$ , (b) the segment with an earthquake with a magnitude  $< 1$ , and (c) the segment with no earthquake. We use  $n = 2000$ ,  $\omega \leq 0.25 \times 2\pi$ , and  $\tau = 0.05, 0.07, \dots, 0.95$  in this experiment.

connected (FC) layer after flattening the output. We include a dropout layer with a rate of 50% to the FC layer, leading to the output layer. The total number of trainable parameters is 2,817,682, and the learning rate is set to be  $1e-4$  with a reduction rate of 0.5 every 20 epochs. Additional details about the model are presented at <https://github.com/tianbochen1>. The model structure

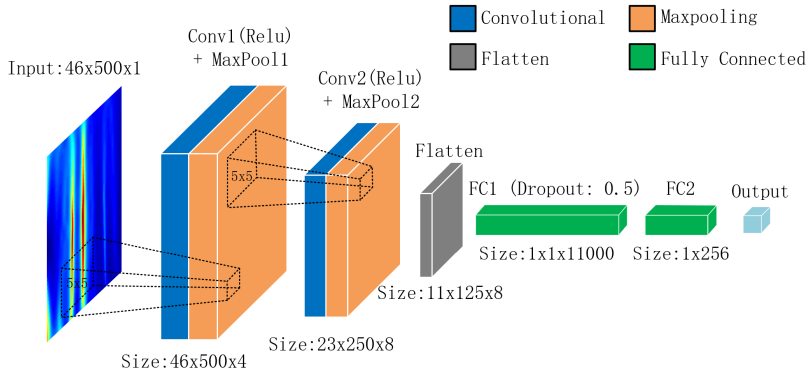


Figure 8: Structure of the deep learning model.

is illustrated in Figure 8. For classifying the ordinary periodograms, which are one-dimensional with respect to  $\omega$ , we adapt the model to use different input dimensions ( $1 \times 500$  instead of  $46 \times 500$ ) and kernel size ( $1 \times 5$  instead of  $5 \times 5$ ).

We conduct the training ten times, randomly constructing the training-testing split and initializing weights using random seeds. Over 80% of the training procedures converge within 30 epochs. The testing accuracy of the three types of periodograms are: expectile periodograms:  $\{0.9900, 1.0000, 0.9925, 1.0000, 0.9975, 0.9950, 0.9925, 0.9925, 0.9950, 0.9925\}$ , quantile periodograms:  $\{0.9825, 0.9900, 0.9925, 0.9925, 0.9825, 0.9950, 0.9925, 0.9900, 0.9875, 0.9825\}$ , and ordinary periodogram:  $\{0.9875, 0.9725, 0.9825, 0.9825, 0.9975, 0.9850, 0.9850, 0.9825, 0.9775, 0.9900\}$ .

The averaged confusion matrices are shown in Table 2, in which true positive (TP) indicates that a segment with an earthquake is correctly classified as having an earthquake, true negative (TN) indicates that the segment without an earthquake is correctly classified as not having an earthquake; false positive (FP) indicates that a segment without an earthquake is incorrectly classified as having one; and false negative (FN) indicates that a segment with an earthquake is incorrectly classified as not having one (where P denotes positive, N denotes negative, T denotes true, and F denotes false).

Table 3 shows three classification metrics: accuracy, precision ( $\frac{TP}{TP+FP}$ ), and recall ( $\frac{TP}{TP+FN}$ ). The optimal value in each row for the three types of periodograms is highlighted in bold. Additionally, We also present the time required for estimation and training (per epoch) to compare the computational complexity of the expectile and quantile periodograms. All computations run on a PC equipped with an Intel Core i9-13900KF processor @5.2GHz, 64 GB of memory, and an Nvidia RTX 4090 graphics card.

Table 2: The averaged confusion matrices of the classification.

(a) Expectile odogram	Peri-		(b) Quantile odogram	Peri-		(c) Ordinary odogram	Peri-	
	P	N		P	N		P	N
T	199.3	198.6	T	196.2	199.3	T	196.2	197.5
F	0.7	1.4	F	3.8	0.7	F	3.8	2.5

Table 3: The classification results.

Metrics		Expectile	Quantile	Ordinary
Accuracy	Averaged	<b>0.9948</b>	0.9880	0.9858
	[min, max]	<b>[0.9925, 1.0000]</b>	[0.9725, 0.9950]	[0.9750, 0.9925]
Precision	Averaged	<b>0.9965</b>	0.9840	0.9843
	[min, max]	<b>[0.9896, 1.0000]</b>	[0.9559, 0.9952]	[0.9609, 0.9902]
Recall	Averaged	<b>0.9931</b>	0.9921	0.9877
	[min, max]	<b>[0.9858, 1.0000]</b>	[0.9794, 1.0000]	[0.9653, 1.0000]
Time (s)	Estimation	12.6684	15.4528	–
	Training	0.3739	0.3731	–

From the results, we can see that

- The classification based on expectile periodograms has higher testing accuracy, precision, and recall rate than the quantile periodograms and the

ordinary periodograms. Specifically, all the testing accuracy in the ten experiments reach 0.99, and two of them are 1. This indicates that the expectile periodograms are suitable features for time series classification.

- One misclassification case in FN using the expectile periodograms is shown in Figure 9. Since the magnitude is too small ( $< 0.1$ ), the power at low frequencies is not as large as the power at high frequencies, which causes the misclassification.
- The expectile periodograms incur a lower estimation complexity compared with the quantile periodograms. However, the computational cost is higher than that of the ordinary periodograms, since the dimension is multiplied by the number of expectile levels.

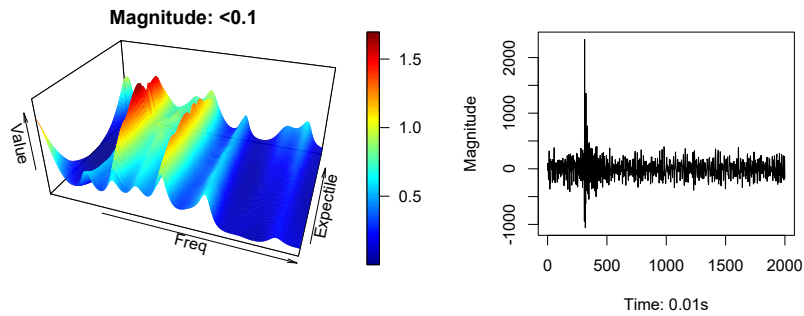


Figure 9: A misclassification case of FN.

## 5. Conclusion

In this paper, we propose the expectile periodograms, a new frequency domain estimator constructed from trigonometric expectile regression. The expectile periodograms exhibit properties analogous to the quantile periodograms, while being distinguished by their high computational efficiency. The expectile periodograms offer more information than the ordinary periodogram by examining the serial dependence at different expectile levels. We conduct real-world examples and simulation studies to highlight their proficiency in detecting

hidden periodicities within time series. In the earthquake data classification task, we leverage the inherent two-dimensional characteristics of expectile periodograms using the deep learning model, which is a powerful technique in image classification.

Nevertheless, the expectile periodograms incurs a higher computational cost in classification and other applications compared to the ordinary periodograms. This computational burden arises from the fact that the dimensionality of the estimator is multiplied by the number of expectiles employed. As illustrated in Section 4.2, Table 3 reveals a substantial contrast in training times per epoch between the expectile periodograms and ordinary periodograms. Specifically, the training time using expectile periodograms amounts to 0.3739 seconds, while it is only 0.1042 when using the ordinary periodograms. One solution to reduce this computational cost is to use fewer expectiles. In this paper, we choose a large number of expectiles uniformly across  $(0, 1)$ . Researchers may choose to focus exclusively on a subset of expectiles with sufficient discriminative power (e.g., high or low expectiles). Furthermore, we utilize multi-thread parallelization to speed up computation using the package `foreach`, `doParallel` in R. The code for reproducing the results in Section 3 (R) and Section 4 (Python) is accessible at [https://github.com/tianbochen1/expectile\\_periodograms](https://github.com/tianbochen1/expectile_periodograms).

### **Acknowledgment**

This work was supported by the National Natural Science Foundation of China under Grant No.12301326, Anhui Provincial Natural Science Foundation under Grant No.2308085QA05, and the University Natural Science Research Project of Anhui Province under Grant No.2023AH050099.

### **References**

- Aigner, D. J., Amemiya, T., and Poirier, D. J. (1976). On the estimation of production frontiers: maximum likelihood estimation of the parameters of a discontinuous density function. *International economic review*, pages 377–396.
- Alvarado, R., Tillaguango, B., Dagar, V., Ahmad, M., Işık, C., Méndez, P.,

- and Toledo, E. (2021). Ecological footprint, economic complexity and natural resources rents in latin america: empirical evidence using quantile regressions. *Journal of Cleaner Production*, 318:128585.
- Baud, M. O., Kleen, J. K., Mirro, E. A., Andrechak, J. C., King-Stephens, D., Chang, E. F., and Rao, V. R. (2018). Multi-day rhythms modulate seizure risk in epilepsy. *Nature communications*, 9(1):88.
- Benz, H. M., McMahon, N. D., Aster, R. C., McNamara, D. E., and Harris, D. B. (2015). Hundreds of earthquakes per day: The 2014 guthrie, oklahoma, earthquake sequence. *Seismological Research Letters*, 86(5):1318–1325.
- Birr, S., Volgushev, S., Kley, T., Dette, H., and Hallin, M. (2017). Quantile spectral analysis for locally stationary time series. *Journal of the Royal Statistical Society: Series B (Statistical Methodology)*, 79(5):1619–1643.
- Bloomfield, P. (2004). *Fourier analysis of time series: an introduction*. John Wiley & Sons.
- Bollerslev, T. (1986). Generalized autoregressive conditional heteroskedasticity. *Journal of econometrics*, 31(3):307–327.
- Brockwell, P. J. and Davis, R. A. (1991). *Time Series: Theory and Methods*. Springer.
- Cai, Z. and Xiao, Z. (2012). Semiparametric quantile regression estimation in dynamic models with partially varying coefficients. *Journal of Econometrics*, 167(2):413–425.
- Cai, Z. and Xu, X. (2008). Nonparametric quantile estimations for dynamic smooth coefficient models. *Journal of the American Statistical Association*, 103(484):1595–1608.
- Chen, T., Sun, Y., Euan, C., and Ombao, H. (2021a). Clustering brain signals: A robust approach using functional data ranking. *Journal of Classification*, 38:425–442.

- Chen, T., Sun, Y., and Li, T.-H. (2021b). A semi-parametric estimation method for the quantile spectrum with an application to earthquake classification using convolutional neural network. *Computational Statistics & Data Analysis*, 154:107069.
- Dette, H., Hallin, M., Kley, T., Volgushev, S., et al. (2015). Of copulas, quantiles, ranks and spectra: An  $l_1$  -approach to spectral analysis. *Bernoulli*, 21(2):781–831.
- Efron, B. (1991). Regression percentiles using asymmetric squared error loss. *Statistica Sinica*, pages 93–125.
- Euán, C., Ombao, H., and Ortega, J. (2018). The hierarchical spectral merger algorithm: a new time series clustering procedure. *Journal of Classification*, 35:71–99.
- Garcia, J., Hernández, P. J., and Lopez-Nicolas, A. (2001). How wide is the gap? an investigation of gender wage differences using quantile regression. *Empirical economics*, 26:149–167.
- Granger, C. and Sin, C. (1997). Estimating and forecasting quantiles with asymmetric least squares. Technical report, Working Paper, University of California, San Diego.
- Gu, Y. and Zou, H. (2016). High-dimensional generalizations of asymmetric least squares regression and their applications.
- Hagemann, A. (2013). Robust spectral analysis.
- Jiang, C., Jiang, M., Xu, Q., and Huang, X. (2017). Expectile regression neural network model with applications. *Neurocomputing*, 247:73–86.
- Jiang, Y., Lin, F., and Zhou, Y. (2021). The  $k$  th power expectile regression. *Annals of the Institute of Statistical Mathematics*, 73:83–113.
- Jones, M. C. (1994). Expectiles and  $m$ -quantiles are quantiles. *Statistics & Probability Letters*, 20(2):149–153.

- Kley, T. (2016). Quantile-based spectral analysis in an object-oriented framework and a reference implementation in r: The quantspec package. *Journal of Statistical Software, Articles*, 70(3):1–27.
- Koenker, R. (2005). Quantile regression. *Cambridge University Press*.
- Koenker, R. (2017). Quantile regression: 40 years on. *Annual review of economics*, 9:155–176.
- Koenker, R. and Bassett Jr, G. (1978). Regression quantiles. *Econometrica: journal of the Econometric Society*, pages 33–50.
- Kouretas, G. P., Zarangas, L., et al. (2005). Conditional autoregressive value at risk by regression quantiles: Estimating market risk for major stock markets. Technical report.
- Kullback, S. and Leibler, R. A. (1951). On information and sufficiency. *The annals of mathematical statistics*, 22(1):79–86.
- Li, T.-H. (2008). Laplace periodogram for time series analysis. *Journal of the American Statistical Association*, 103(482):757–768.
- Li, T.-H. (2012a). Detection and estimation of hidden periodicity in asymmetric noise by using quantile periodogram. In *Proceedings of the IEEE International Conference on Acoustics, Speech and Signal Processing (ICASSP)*, vol 2, pp. 3969–3972.
- Li, T.-H. (2012b). Quantile periodograms. *Journal of the American Statistical Association*, 107(498):765–776.
- Li, T.-H. (2014). Quantile periodogram and time-dependent variance. *Journal of Time Series Analysis*, 35(4):322–340.
- Li, T.-H. (2023). Quantile-frequency analysis and deep learning for signal classification. *Journal of Nondestructive Evaluation*, 42(2):40.



- Maadooliat, M., Sun, Y., and Chen, T. (2018). Nonparametric collective spectral density estimation with an application to clustering the brain signals. *To appear in Statistics in Medicine*.
- Machado, J. A. and Mata, J. (2005). Counterfactual decomposition of changes in wage distributions using quantile regression. *Journal of applied Econometrics*, 20(4):445–465.
- Martínez-Murcia, F. J., Ortiz, A., Morales-Ortega, R., López, P., Luque, J. L., Castillo-Barnes, D., Segovia, F., Illan, I. A., Ortega, J., Ramirez, J., et al. (2019). Periodogram connectivity of eeg signals for the detection of dyslexia. In *Understanding the Brain Function and Emotions: 8th International Work-Conference on the Interplay Between Natural and Artificial Computation, IWINAC 2019, Almería, Spain, June 3–7, 2019, Proceedings, Part I 8*, pages 350–359. Springer.
- Meziani, A., Medkour, T., and Djouani, K. (2020). Penalised quantile periodogram for spectral estimation. *Journal of Statistical Planning and Inference*, 207:86–98.
- Newey, W. K. and Powell, J. L. (1987). Asymmetric least squares estimation and testing. *Econometrica: Journal of the Econometric Society*, pages 819–847.
- Polat, K. and Güneş, S. (2007). Classification of epileptiform eeg using a hybrid system based on decision tree classifier and fast fourier transform. *Applied Mathematics and Computation*, 187(2):1017–1026.
- Schnabel, S. K. and PHC, E. (2009). Non-crossing smooth expectile curves. In *Proceedings of the 24th International Workshop on Statistical Modelling. Ithaca, NY, USA*, pages 330–36.
- Sharif, A., Bhattacharya, M., Afshan, S., and Shahbaz, M. (2021). Disaggregated renewable energy sources in mitigating co2 emissions: new evidence from the usa using quantile regressions. *Environmental Science and Pollution Research*, 28(41):57582–57601.

- Shumway, R. H. and Stoffer, D. S. (2016). *Time series analysis and its applications: with R examples*. Springer Science & Business Media.
- Waltrup, L. S., Sobotka, F., Kneib, T., and Kauermann, G. (2015). Expectile and quantile regression—david and goliath? *Statistical Modelling*, 15(5):433–456.
- Xu, Q., Chen, L., Jiang, C., and Yu, K. (2020). Mixed data sampling expectile regression with applications to measuring financial risk. *Economic Modelling*, 91:469–486.
- Yao, Q. and Tong, H. (1996). Asymmetric least squares regression estimation: a nonparametric approach. *Journal of nonparametric statistics*, 6(2-3):273–292.